ONLINE METHODS

Microscope design. Two separate ultrashort-pulsed sources were used for two-photon imaging (Coherent Chameleon Ultra II, 920 ± 6 nm, <200-fs output pulse duration) and for photostimulation (FemtoPower 5W, Fianium; 1,064 ± 6 nm, <300 fs). In experiments with visible-wavelength single-photon stimulation, a diode-pumped solid-state source was used (λ = 473 nm, 100-mW unit, OEM Laser Systems). The 920-nm and 1,064-nm paths were combined using a long-pass dichroic mirror (950dcxrxt, Chroma) and reflected to the microscope focusing objective (LUMPLFLN 40XW, Olympus) using a short-pass dichroic mirror (700dcspxr, Chroma) with good transmission of 473-nm light (for SPE stimulation; **Supplementary Fig. 2**) and excited fluorescence (for imaging). Following an infrared light-blocking filter (FF01-680/SP-25, Semrock), excited fluorescence was separated for two-channel detection using a dichroic mirror (FF518-Di01, Semrock), two emission filters (FF01-494/41 and FF01-578/105, Semrock), two photomultiplier tubes (H10770P-40SEL, Hamamatsu), and a high optical density long-pass edge filter (LP02-473RU, Semrock) to block 473-nm light from the detector assembly. Spectral properties of

molecules, laser sources and optics used in this design are shown together in **Supplementary Figure 1**.

A blazed ruled diffraction grating (#3-4114, UTF-CW series, 1,200 lines per mm, Optometrics) oriented around the Littrow configuration (close to retrodiffraction) was used to shape the spatial profile of pulses from the 1,064-nm source by temporal focusing[16,24,25,51]. Following a 1:1 afocal telescope (focal length f = 300 mm, Thorlabs #AC508-300-C), an aperture (**Fig. 1**) in a plane optically conjugate to the grating was used to reduce the outer diameter of the temporally focused spot. An achromatic doublet (Thorlabs #AC300-100-B) transformed the spot to a spectral line focus in the Fourier plane, which was positioned at the center of a pair of XY galvanometer-driven scanning mirrors (3-mm aperture, 6210 series; Cambridge Technology). Two additional afocal telescopes (f = 63 mm, #4401-387-000-21, Qioptiq; f = 164 mm, #NT58-395, Edmund Optics; f = 160 mm, #G322310525, Qioptiq; f = 200 mm, #58-520, Edmund Optics) were used to map the plane of optical rotation to the entrance pupil of the microscope objective with minimal insertion loss, producing a temporally focused TPE spot profile with appropriate demagnification that could be scanned in the sample plane. The TPE spot profile in the sample plane (**Fig. 1**) was measured near the center of the field of view using a thin fluorescent sample (100 μM Alexa 594 in 3% bovine serum albumin, 1μl spread on coverglass and then air-dried) and an inverted microscope design[52] consisting of a 60× air objective (LUMPLFLN 60XW, Olympus), a long-pass dichroic, infrared blocking and bandpass filters (BG39 glass, Schott; 607/70, Semrock), and a CCD camera (Coolsnap CF, RoperScientific). 1,064-nm power at the sample plane was controlled using a Pockels cell (#350-80 modulator with 302RM driver; Conoptics). For imaging (920 nm), laser power was controlled using an attenuator based on a Berek compensator (W. Denk, US patent 6,249,379 B1 (June 19, 2001)) in a double-pass configuration, and scanning used galvanometer-driven mirrors (6210 series mirrors and 677 Micromax series drivers; Cambridge Technology). Power was monitored throughout experiments using pickoff photodiodes calibrated against through-objective power measurements obtained with a thermal detector (Fieldmaster, Coherent).

The system included four optical paths: imaging (920 nm), primary TPE stimulation (1,064 nm, temporal focusing), secondary TPE stimulation (1,064 nm, spatial focusing) and SPE stimulation (473 nm). Registration of the TPE paths was achieved by adjusting offset voltage to the

scanning mirrors (920-nm and 1,064-nm TF path), optical input angle to the scanning mirrors (1,064-nm SF path), and scanning mirror voltage range to minimize the differences between acquired images of a thin air-dried fluorescent sample on a fiducial grid (Thorlabs #R1L3S3P). Beam divergence of the 920-nm path was adjusted to achieve parfocality with the 1,064-nm paths, using a variable-focus electric liquid lens (EL-10-30, Optotune; 250 mA driver, Thorlabs #LD1255R) with a compound offset lens[53] (f = –100mm; Thorlabs #LC1120-B) positioned in an optical plane approximately conjugate to the scanning-mirror plane in the imaging system (**Fig. 1**). The SPE source was focused in the common TPE scanning plane by alternately bleaching (SPE) and imaging (TPE) the thin fluorescent sample, adjusting lateral and axial position of the SPE focus with an alignment mirror and telescope lenses leading to the entrance port in the microscope head (**Supplementary Fig. 2**).

To eliminate registration errors arising from movement of optics in the microscope (for example, during refocusing) all optics in the system were held in fixed positions, whereas movement and refocusing instead used a custom-built stage to translate the sample itself. The stage consisted of a two-axis linear translation table (XYR-8080, Dover-Danaher) and two mechanically coupled vertical translation stages (MVN80, Newport; Flex-E-Belt system, W.M. Berg) supporting a platform on which a styrofoam treadmill and headplate holders were mounted. Motorized movements of the sample platform in all three dimensions (x, y and z) were actuated using a modified MP285 microcontroller (v. DT3.3, Sutter Instruments).

Instrument control and data acquisition. The instrument was controlled using custom virtual instrument panels written in LabView (National Instruments). Signal acquisition and generation for two analog input channels and six analog output channels (two pairs of *XY* scanning mirrors, plus Pockels cell control and an auxillary output) used three acquisition boards (PCI-6110E, PCI-6221 and PCIe-6321; National Instruments) synchronized using the Real Time System Integration bus (National Instruments). In some experiments, stimulation periods were gated using analog outputs generated by a Digidata 1440A and Clampex v.10 (Molecular Devices), using the shutter sync signal from the laser shutter driver (#VMM-D1 with LS6ZM2 shutter, Vincent Associates) to trigger waveform generation. In some experiments, ScanImage software[54] was used for image acquisitions.

Measurements to characterize the response properties of illuminated neurons (**Figs. 2** and **3**) were obtained in awake, mobile mice that were not in a VR environment. In all of these experiments, an interval of at least 60 s was enforced between repeat trials to stimulate any one cell. Protocols varying one stimulation parameter (for example, laser power or target location) were performed in blocks consisting of interleaved trials of most or all types and including at least one reference trial. For example, a measurement of in-plane spatial resolution (as in **Fig. 3a**) consisting of an on-target trial (T) and four trials at different positions offset from the cell ($\pm X$ and $\pm Y$) would be arranged as: (T, $+X$, $-Y$, $+Y$, $-X$, T, $-Y$, $+X$, $+Y$, $-X$,...). Cells were selected on the basis of visibility and expected responsiveness to stimulation (cytoplasmic GCaMP fluorescence, and high EYFP brightness defining the nucleus). In experiments where multiple cells were selected for stimulation from a single field of view during awake imaging sessions, neurons were selected based on visibility of the in-plane soma (typically, a donut-like GCaMP3 fluorescence) and volume-filling EYFP fluorescence (indicating C1V1 expression), without considering distance between targets. As such, targeted neurons were distributed around the field of view, including some that were very close and others that were more widely separated (see **Fig. 3c**).

To obtain a stimulation and imaging time series, an acquired image was viewed online and used to select the center locations of one or more targets (cell somas) manually (LabView Image Acquisition Toolbox). The (x,y) scanner offset voltage values were computed from the (x,y) pixel coordinates of each target. Then, an image acquisition was initiated and several frames into the acquisition (typically 4–8 or 0.25–0.5 s at ~16-Hz acquisition rate), a photostimulation protocol was initiated. Fluorescence images were acquired continuously during the stimulation epoch (typical duration $\leq$ 1 s) and ended 1–5 s later. During a stimulation and imaging time series, 1,064-nm photostimulation exposure timing was controlled using a Pockels cell modulated between 'off' (extinction ratio > 400:1) and 'on' (the power setpoint) at high bandwidth (≈10 kHz) by analog command steps gated by a MOSFET switch, using start triggers generated by the instrument control software (LabView). Visible-wavelength stimulation exposures (**Fig. 3a**,**b**) were controlled using TTL pulses to modulate laser output power at the supply. Stimulation trials used 1,064-nm TPE that was either temporally focused (**Fig. 1**, TF) or conventionally focused (spatial focusing, SF). In single-cell SF experiments, a low-NA focus (≈0.3NA) generated by underfilling the objective was rapidly scanned over the target (typical dimensions ≈12–15 μm, scan period of 8–16

ms, sinusoidal raster-pattern). In single-cell TF experiments, the spot occupied a fixed position centered on the target. In multiple-cell experiments of either type, the illumination profile was repositioned to target a sequence of locations.

Spatial resolution measurements using TPE and SPE (**Fig. 3**) were obtained by acquiring a stimulation and imaging time series where the target was centered on a cell of interest, and then translating the stage to a different position (x, y or z) and acquiring another time series. When the z value was changed (along optical axis), the imaging system was refocused at the original plane of the target cell using a liquid lens. Additional spatial resolution measurements using only TPE were obtained from groups of targeted cells; these time series were acquired sequentially, repositioning the illumination profile (rather than the sample) to target each neuron, and allowing at least 2 s between stimulation epochs targeting different cells (60 s between epochs targeting the same cells).

For experiments in behaving mice (during VR environment interaction), stimulation and imaging time series were synchronized with behavior by recording the imaging path shutter sync signals (as file markers) and scanning mirror command signals (acquisition end markers) along with current VR environment position, traversal number, running speed, reward timing and the gate signal used to modulate stimulation exposure epochs in ViRMEn software (see below). In experiments using ScanImage for image acquisition, an analog voltage signal encoding position in the VR environment was recorded on the third channel in the imaging time series. Photostimulation trials targeting single cells during VR navigation used 10-Hz pulses (50-ms duration), and were performed in an alternating sequence with imaging-only trials (trials were traversals of the environment; reward delivery toggled between trial-types) during periods when the mouse was running in the environment (instantaneous ball velocity >0.5 cm s^{-1}). In VR location–specific stimulation trials (**Fig. 4**), ViRMEn software was used to enable the pulse train controlling stimulation exposures only when the mouse's position in the VR environment was in the designated region (**Fig. 4**). For optical bias stimulation (**Fig. 5**), the stimulation pulse train was enabled at all locations in the environment.

Mouse surgical procedures and behavior training. All experiments were performed in compliance with the Guide for the Care and Use of Laboratory Animals, and protocols approved by the Princeton University Institutional Animal Care and Use Committee. Heterozygous male *Thy1-GCaMP3-WPRE* transgenic mice (strain GP2.11; provided by D.S. Kim, Genetically Encoded

Neuronal Indicator and Effector Project, Janelia Research Campus) were used in all experiments unless otherwise noted. Surgical procedures for virus injection and chronic implantation of a headplate and optical imaging window used methods described previously[3], but were modified in the following ways: the viral vector used for injections was rAAV5 carrying the *Camk2a::C1V1(t/t)-TS-P2A-EYFP* expression cassette (1.6×10^{13} GC ml^{-1}; Gene Therapy Center, University of North Carolina at Chapel Hill), 500–650 nl of virus solution was injected over a period of 10–15 min, and headplate implantation occurred in the same surgical procedure as injection. Mice were 8–10 weeks old at the time of surgery and were housed in groups (3–4 mice per cage) in a vivarium on a reverse light-dark cycle.

Mice were trained during the day to run on a linear track in a visual VR environment using a VR projection system and behavior training procedures (including water scheduling) described previously[3,30,55], but modified in the following ways. First, animal handling, acclimation to the treadmill and water scheduling (1 ml/day) began >3–4 d after the optical window implantation surgery and VR training began around 7 d after surgery. Second, mice were trained to run along a unidirectional 400-cm-long virtual linear track as described[55], but using an air-supported styrofoam treadmill constrained to rotate about one axis (pitch) and an optical mouse to detect movements[56]. Mice adapted quickly to this approach, running for many rewards (>100 per h) within 1–2 weeks of initiating training. Third, VR-based behavior experiments were designed and executed using a general-purpose software system (Virtual Reality Matlab Engine, or ViRMEn[29]). Using ViRMEn, properties of ongoing behavior (such as environment position or reward number) were used to compute custom gate signals, which were written as high or low voltages to a NI-DAQ analog output channel with each environment update cycle (~30–35 ms) and used to synchronize stimulation with specific epochs in the behavior. Finally, environment projection used a blue bandpass filter (455/110, Chroma) and a toroidal projection surface as described[3,30], but which was machined from expanded polystyrene (1.5# eps; Global Manufacturing Solutions) and coated with reflective paint to increase environment brightness. The screen was also constructed of 3 90-degree segments joined by hinges to allow experimental access to the stage without moving the microscope.

Data analysis. Data were analyzed using toolboxes and custom scripts written in Matlab (R2012a; Mathworks). For all experiments, two-channel imaging time series acquisitions were first separated

into estimated GCaMP and YFP time series using linear unmixing adapted from a method that has been described[57]. In two-channel linear unmixing, two detectors with different spectral bandpass filters are used to measure the combined fluorescence from two types of fluorophore with overlapping emission spectra, using the unique ratio of detector signals for each fluorophore alone (its spectral signature) to estimate the ratio of fluorophore concentrations[26]. Here, the spectral signatures of GCaMP and EYFP were measured using the same imaging preparation (hippocampal window) in wild-type C57/BL6 mice (Jackson Laboratories) with virally mediated expression of either GCaMP6[36] (*AAV1-Syn::GCaMP6s-WPRE-SV40*, $3x10^{13}$ GC ml^{-1}, 100-nl injection volume; University of Pennsylvania Vector Core) or C1V1(t/t)-2A-EYFP. These detector signal ratios (0.33:1 and 1:150, with this filter set) were then used to unmix time series acquisitions by file (that is, as a time-independent block of pixels) after subtracting the measured PMT pre-amplifier offset for each channel. This yielded two time series, GCaMP and YFP, for each acquisition. In principle, differences in background between the reference measurement and data sets could cause errors in unmixing, but in practice, cells in the unmixed GCaMP data sets appeared nuclearly excluded and showed normal calcium-dependent fluorescence transients (**Supplementary Fig. 3**), whereas cells in the unmixed YFP data sets appeared volume-filled and did not show fluorescence transients (**Fig. 2**). The same offset and detector ratios were used for all data sets.

GCaMP and YFP time series were motion-corrected together, using one set of full-frame centroid-shifts computed by cross-correlation[58] of the GCaMP time series. Slow changes in full-frame fluorescence over long recordings were compensated by computing the distribution of all pixel intensities in 15-s blocks and subtracting the eighth percentile value from those frames. Regions of interest (ROIs) in motion-corrected GCaMP data sets were identified manually[56] or by using an automated approach[59] ($\mu = 0.5–1$)[3], and $\Delta F/F$ traces were computed for each ROI. In a few cases where specific cells of interest were not identified by the automated algorithm, $\Delta F/F$ traces were computed from manually selected ROIs and appended to the population data set. For experiments using SPE stimulation, where blue-light pulses were synchronized with periods of transient detector saturation (bright groups of lines in the image), lines in stimulation frames that exceeded the median line-by-line fluorescence across all epochs (at the time in the stimulation epoch) by >1% of the s.d. were excluded from calculation of $\Delta F/F$ values. Significant transients were identified in baseline-corrected traces as periods where $\Delta F/F$ values increased to cross a

threshold value of 3 σ_s above the median value and remained continuously above a value of 0.5 σ_s for at least 0.5 s. Here, σ_s is the median of all s.d. computed for the full $\Delta F/F$ trace in 1–2-s bins; this approach gave reasonable estimates of baseline fluorescence even under conditions of large and/or frequent transients. In significant transient-only traces, the significant transients were unmodified, and the values at time points between significant transients were set to zero[3,56,60]. $\Delta F/F$ traces were used for further analysis in experiments, except where indicated.

YFP traces marking 1,064-nm stimulation epochs (as in **Fig. 2c**) were computed using YFP data sets that were analyzed as a time series of pixels in the order that they were acquired (rather than as frames) during stimulation trials. These traces represent whole field–detected YFP fluorescence in time, smoothed using a first-order Savitsky-Golay filter (16-ms window) and averaged across three or more stimulation trials. YFP/GCaMP fluorescence ratios (as in **Fig. 2d**) represent the ratio of unmixed YFP fluorescence in each cell to unmixed resting GCaMP fluorescence in all cells in that field of view. For each cell in a given field of view, the YFP/GCaMP fluorescence ratio was computed as the mean YFP fluorescence across all pixels in the ROI for that cell and all frames in the acquisition (after excluding frames where the cell had significant GCaMP transients) divided by the GCaMP fluorescence in all cells (full-field median) from the same frames, at the same input laser power. A spontaneous event (as in **Fig. 2d**) was defined as a significant transient detected in a neuron-ROI during 920-nm imaging with the 1,064-nm laser blocked. Rates of spontaneous events were calculated for each ROI by summing the number of significant transients observed across all recordings at each laser power, and then dividing that number by the total recording time (in seconds) at that laser power. Spontaneous event rates for all ROIs were then averaged across groups of cells binned by YFP/GCaMP ratios.

In single-cell stimulation spatial resolution measurements (as in **Fig. 3a**–**c**), $\Delta F/F$ traces were calculated for all cells in each field of view that were selected as targets for stimulation. Those cells were considered responsive to stimulation if a significant transient occurred in a 1-s interval around stimulation onset, using a value of 4 σ_s for the threshold change at onset to classify transient changes as significant, the peak transient amplitude in that interval was >25% $\Delta F/F$, and significant transients occurred at least twice across all trial intervals (trials were typically repeated 5–10 times). To determine the fraction of experiments in which any neuron other than the targeted neuron responded to stimulation, additional ROIs were defined (947 in total, across 16 FOVs) and

the analysis above was repeated to compute additional $\Delta F/F$ traces and then identify stimulation-triggered responses in all ROIs (in addition to stimulation-targeted cells). Two additional steps were taken to reduce false positive detection resulting from spillover (fluorescence transients originating in somas in adjacent, partially overlapping ROIs). First, ROIs that were not targeted, but which responded to stimulation (according to the three criteria described above), were identified as candidate off-target responders. If any single trial produced a response in the candidate ROI without also producing a response in the target ROI, the candidate ROI was automatically designated as an off-target responding neuron. If responses in the candidate ROI only occurred in trials where the target neuron also responded, then the time series was inspected manually to determine whether the $\Delta F/F$ signal detected in the candidate ROI originated in that neuron or the targeted neuron.

For recordings during VR behavior, periods in which the mouse was stationary (ball velocity < 0.5 cm s^{-1}) were excluded from analysis. Cells with task-modulated activity were classified using an adaptation of an approach described previously[3]. First, traversals of the environment were divided into two trial-types: off trials (no photostimulation; imaging only) or on trials (all biasing stimulation trials, or direct stimulation trials where place-specific stimulation produced a transient in that cell). For each category and each cell, $\Delta F/F$ values were calculated as a function of VR spatial location by averaging over 7.5-cm spatial bins in each traversal. The mean spatially binned $\Delta F/F$ across all traversals in that category was then computed. If the peak $\Delta F/F$ value in this trace was located in a region of contiguous activity (>0.25 times the peak for ≥30 cm), this region was considered a candidate place field. If the mean in-field $\Delta F/F$ contained one value of at least 0.1 and significant transients were present at least 20% of the time spent running in that field in individual traversals, the cell was classified as having a place field in that trial type. Cells with place fields in off trials were classified as place cells.

Factor analysis (ten factors) was performed using a Matlab toolbox and custom scripts. Variables for factor analysis consisted of place cells (ROIs from imaging time series), and observations consisted of spatially binned $\Delta F/F$ traces from early (15–25 cm) in traversals up to the water reward (360 cm). For all cells, activity traces across single traversals were concatenated across off trials and then across an equal number of on trials. Each column in the matrix (observations for one cell) was then smoothed using a window of three spatial bins (22.5 cm) and

divided by the maximum value in the column. Factor analysis was performed once using all place cells (including the cell or cells targeted for stimulation) and then repeated after removing the target cell(s) from the matrix. Trajectories were plotted using the first three common factors. The distance between trajectories represents the Euclidean distance in the factor space at each VR spatial bin center.

No calculation was performed to determine sample size a priori; sample sizes were chosen to be similar to previous studies characterizing optical stimulation (tens of stimulated cells) and analyzing *in vivo* fluorescence recordings (hundreds). Bootstrap resampling was used to evaluate statistical significance of differences in spatially modulated activity ($\Delta F/F$ traces from single cells) between on or off trial types. For each cell, equal numbers of single-traversal $\Delta F/F$ traces from each trial-type were shuffled and sampled (with replacement) and used to compute two mean $\Delta F/F$ traces. Then, the absolute value of the difference between the summed fluorescence for each mean trace (area under each curve) was computed. This process was repeated at least 100,000 times to produce a distribution of this quantity. This distribution was then used to assign a *P* value for the same quantity computed using the original (unshuffled) traces. To estimate false discovery rate using this approach, the procedure was repeated after shuffling and sampling (with replacement) trial-type labels (on or off). The distribution of *P* values computed in this way (repeated to obtain at least 200 *P* values) in data sets where this test was applied was approximately uniform between 0 and 1 (that is, with 4–5% of *P* values below 0.05; two data sets). The same approach was used to evaluate significance of Euclidean distances between mean state-space trajectories (single-trial trajectories computed using factor analysis; see above). Correlation coefficients between place fields in different cells were computed using the first half of the matrix used for factor analysis (off trials only), and Matlab's *corrcoef* function.

51. Vaziri, A. & Emiliani, V. Reshaping the optical dimension in optogenetics. *Curr. Opin. Neurobiol.* **22**, 128–137 (2012).

52. Dana, H. & Shoham, S. Numerical evaluation of temporal focusing characteristics in transparent and scattering media. *Opt. Express* **19**, 4937–4948 (2011).

53. Grewe, B.F., Voigt, F.F., van 't Hoff, M. & Helmchen, F. Fast two-layer two-photon imaging of neuronal cell populations using an electrically tunable lens. *Biomed. Opt. Express* **2**, 2035–2046 (2011).

54. Pologruto, T.A., Sabatini, B.L. & Svoboda, K. ScanImage: flexible software for operating laser scanning microscopes. *Biomed. Eng. Online* **2**, 13 (2003).

55. Domnisoru, C., Kinkhabwala, A.A. & Tank, D.W. Membrane potential dynamics of grid cells. *Nature* **495**, 199–204 (2013).

56. Harvey, C.D., Coen, P. & Tank, D.W. Choice-specific sequences in parietal cortex during a virtual-navigation decision task. *Nature* **484**, 62–68 (2012).

57. Zimmermann, T., Rietdorf, J., Girod, A., Georget, V. & Pepperkok, R. Spectral imaging and linear un-mixing enables improved FRET efficiency with a novel GFP2-YFP FRET pair. *FEBS Lett.* **531**, 245–249 (2002).

58. Miri, A., Daie, K., Burdine, R.D., Aksay, E. & Tank, D.W. Regression-based identification of behavior-encoding neurons during large-scale optical imaging of neural activity at cellular resolution. *J. Neurophysiol.* **105**, 964–980 (2011).

59. Mukamel, E.A., Nimmerjahn, A. & Schnitzer, M.J. Automated analysis of cellular signals from large-scale calcium imaging data. *Neuron* **63**, 747–760 (2009).

60. Dombeck, D.A., Graziano, M.S. & Tank, D.W. Functional clustering of neurons in motor cortex determined by cellular resolution imaging in awake behaving mice. *J. Neurosci.* **29**, 13751–13760 (2009).

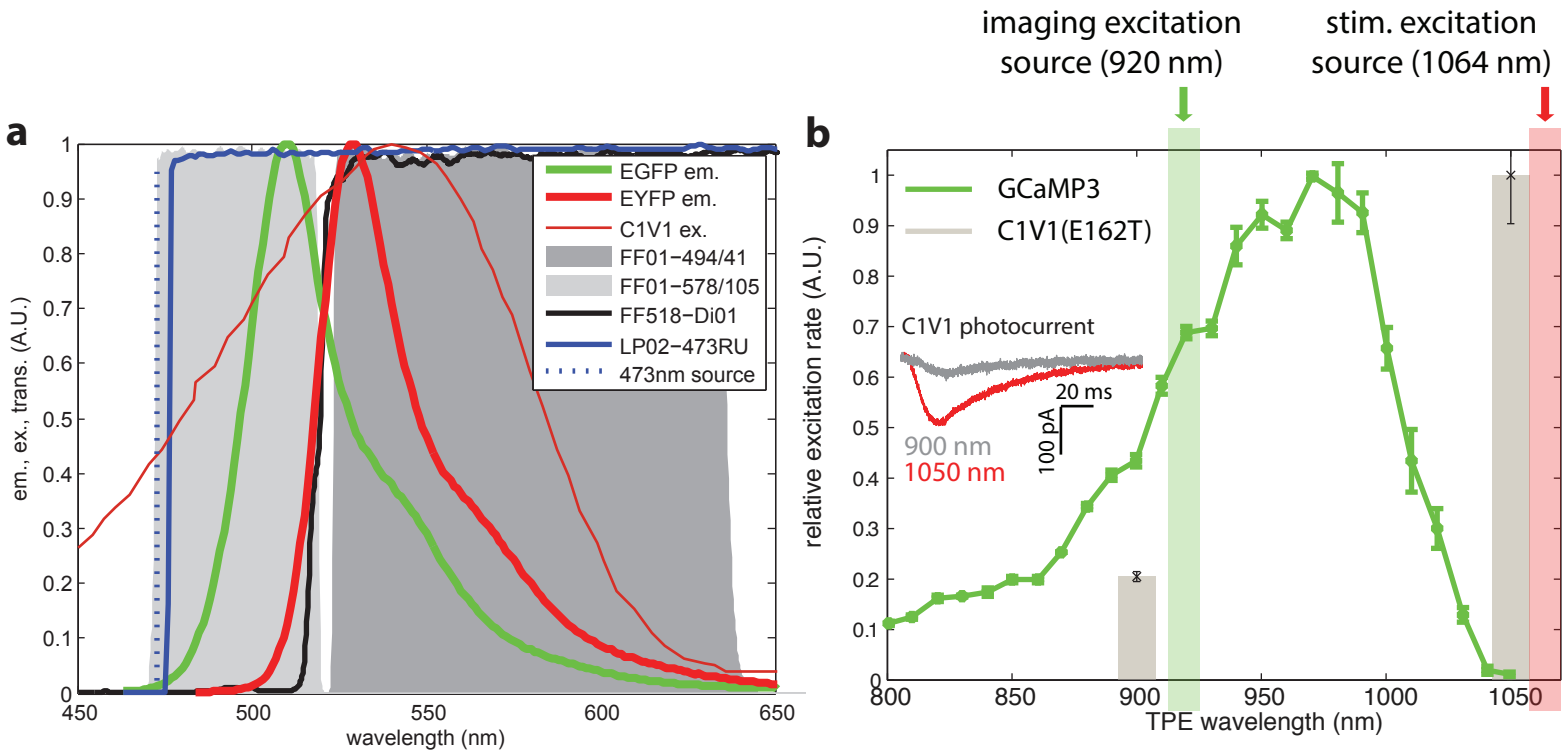

Supplementary Figure 1. Spectral properties of molecules, laser sources, and optics used in this approach.

a. Visible-wavelength regime. Shown are: fluorescence emission spectra for EGFP and EYFP (obtained from the Tsien Lab website, University of California, San Diego); the single-photon excitation spectrum for C1V1(E122T/E162T) (adapted from Yizhar et al., *Nature* 477, 171-178 [2011]); transmission curves for the dichroic (dark line) and emission filters (shaded areas) used in two-channel fluorescence detection (filter part numbers indicated); and the transmission curve for the long-pass laser-blocking filter (blue line; curves from Semrock). The 473 nm laser line used in single-photon excitation experiments is also indicated (dashed blue line). Each curve is normalized to its own peak value.

b. Infrared-wavelength regime. Two-photon action cross section for GCaMP3 (green) and relative C1V1 photocurrent response amplitudes (see inset) sampled at two infrared TPE center wavelengths (λ=900 nm and λ=1050 nm). Inset: sample intracellular photocurrents from illuminated HEK293T cells expressing C1V1; peak squared-intensity values were similar (2.76×10^{54} $\gamma^2/cm^4\text{-}s^2$ and 1.68×10^{54} $\gamma^2/cm^4\text{-}s^2$ at 900 nm and 1050 nm; assuming a fixed output temporal pulse-width). The GCaMP3 action cross-section was measured using fluorescence excited by focused low-power illumination (regime of quadratic power dependence) of a purified GCaMP3.3 sample (37 μM concentration in 20 mM MOPS, 100 mM KCl, 2.7 mM K_2CaEGTA, at pH 7.4; R. Sun and S. S.-H. Wang, Princeton), normalized at each wavelength using side-by-side measurements of a reference fluorophore (20 μM fluorescein in water, pH 11; see Albota, M. A., Xu, C. & Webb, W., *Appl. Opt.* 37, 7352–7356 [1998]). C1V1 wavelength-sensitivity was evaluated at two spectral bands (λ=900 nm and 1050 nm), using whole-cell electrode recordings at constant voltage (-50 mV) in HEK293T cells transiently expressing the pLenti-CaMKIIa-C1V1(E162T)-TS-EYFP construct with focused scanning methods and an apparatus described previously (Rickgauer and Tank, *PNAS* 106, 15025-15030 [2009]).

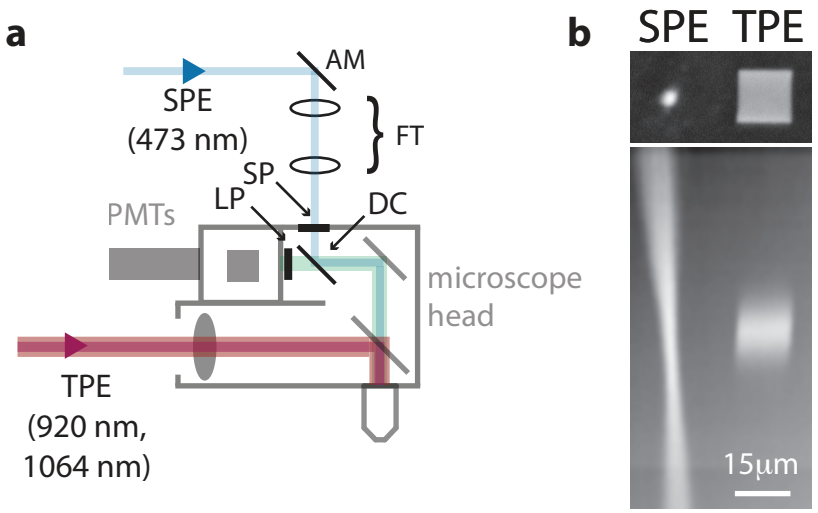

Supplementary Figure 2. Schematic for either single-photon or two-photon excitation (TPE) photostimulation and TPE imaging.

a. Position of optics used to introduce the SPE source into the TPE microscope head. Abbreviations: AM, alignment mirror; FT, focusing telescope; SP, short-pass filter; DC, dichroic filter; LP, long-pass filter; PMTs, photomultiplier tubes.

b. TPE images (acquired at 920 nm) of a volume in a fluorescent plastic slide after bleaching neighboring areas using SPE (473 nm) and TPE (1064 nm, spatial focusing path; SF in Fig. 1, main text). Image intensity is inverted. Images are shown at the 1064 nm focal plane (upper) and as an xz projection of a through-focus series (lower).

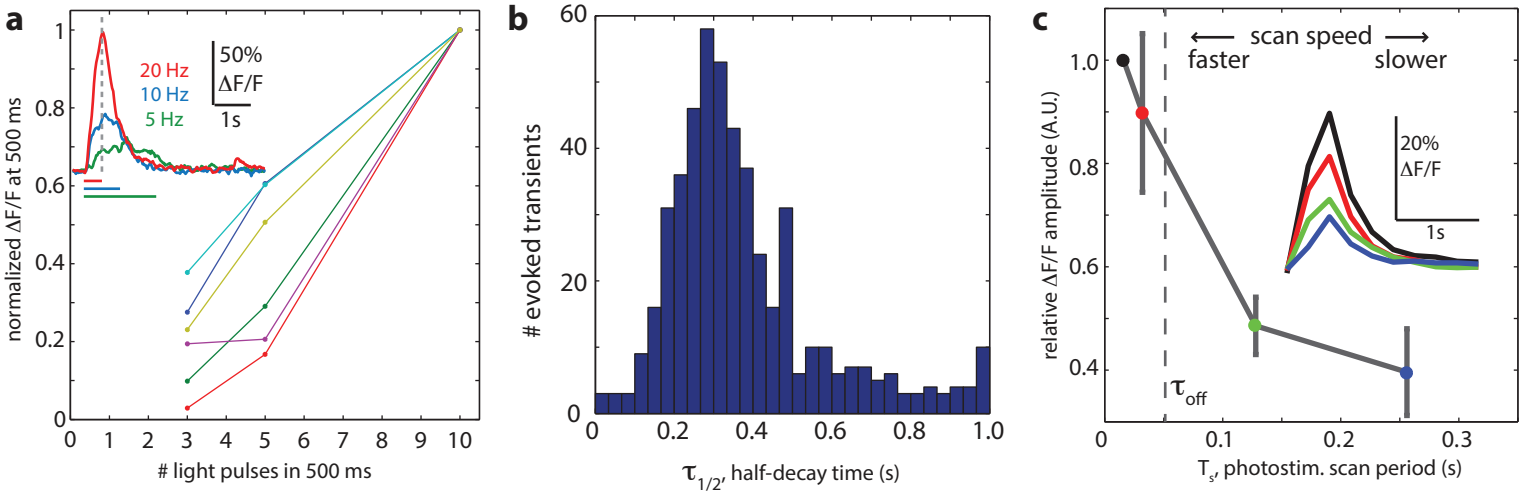

Supplementary Figure 3. TPE stimulation evokes GCaMP3 transients consistent with action potentials (APs) and opsin-mediated depolarization in awake mice.

a. GCaMP3 ΔF/F values vs. stimulation pulse number. Somatic ΔF/F values for 6 neurons stimulated at 5, 10, and 20 Hz (16 ms per pulse), measured 500 ms after pulse-train onset (values for each cell are normalized to the peak response; average of 3-7 trials per data point). The monotonic relationship between ΔF/F and stimulation pulse number is consistent with a regime in which ΔF/F values also scale approximately linearly with AP number (assuming 1 AP per pulse; Tian et al., *Nat. Methods* 6, 875-881 [2009]). Inset: sample traces from one neuron stimulated with 10 pulses at 5, 10, and 20 Hz (each trace is a 5-trial average). Colored underlines indicate the corresponding stim. train period. Dashed line indicates the time at which values ΔF/F values were measured (500 ms after stim. onset).

b. Histogram of measured GCaMP3 fluorescence transient half-decay times following offset of a photostimulation epoch ($\tau_{1/2}$ calculated from single-exponential decay fits). Following stim. offset, transients evoked in cells returned to resting levels with off-kinetics ($\tau_{1/2}$ = 375 +/- 196 ms; mean +/- s.d.) in the range observed *in vivo* during trains of electrically stimulated APs ($\tau_{1/2}$ = 384 +/- 76 ms for 10 APs; Tian et al., *Nat. Methods* 6, 875-881 [2009]).

c. Peak GCaMP3 transient amplitude during raster-scanning photostimulation of a cell using the spatial focusing path (SF in Fig. 1, main text) shown for different TPE raster-scan periods, which varied by changing the number of lines in a raster-scan, and which were repeated over an interval of 512 ms. The dashed line indicates the approximate C1V1(t/t) inactivation time-constant (τ_{off} = 40-50 ms; Mattis et al., *Nat. Methods* 9, 159-172 [2012]; Prakash et al., *Nat. Methods* 9, 1171-1179 [2012]). Faster-scanning photostimulation trials ($T_s < \tau_{off}$) produced larger-amplitude responses than slower-scanning trials ($T_s > \tau_{off}$; n=31 target cells; values for each cell normalized by maximum amplitude in that cell). This relationship is a signature of membrane depolarization mediated by scanning recruitment of opsin probes (Rickgauer and Tank, *PNAS* 106, 15025-15030 [2009]; Prakash et al., *Nat. Methods* 9, 1171-1179 [2012]; Packer et al., *Nat. Methods* 9, 1202-1205 [2012]). Inset: Exemplary ΔF/F traces from one cell illustrating this relationship (colors indicate scan periods of same-color dots in panel; bars indicate s.d.).